

1 **Estimation of PM10 concentrations over Seoul using**  
2 **multiple empirical models with AERONET and MODIS data**  
3 **collected during the DRAGON-Asia campaign**

4  
5 **Sora Seo<sup>1,\*</sup>, Jhoon Kim<sup>1</sup>, Hanlim Lee<sup>1,2</sup>, Ukkyo Jeong<sup>1</sup>, Woogyung Kim<sup>1</sup>, Brent N.**  
6 **Holben<sup>3</sup>, Sang-woo Kim<sup>4</sup>, Chul H. Song<sup>5</sup>, and Jaehyeon Lim<sup>6</sup>**

7 [1]{Institute of Earth, Astronomy, and Atmosphere, Brain Korea 21 Plus Program,  
8 Department of Atmospheric Sciences, Yonsei University, Seoul, Republic of Korea}

9 [2]{Department of Spatial Information Engineering, Pukyong National University, Busan,  
10 Korea}

11 [3]{NASA Goddard Space Flight Center, Greenbelt, MD, USA}

12 [4]{School of Earth and Environmental Sciences, Seoul National University, Seoul, Korea}

13 [5]{Department of Environmental Engineering, GIST, Gwangju, Korea}

14 [6]{National Institute of Environmental Research, Incheon, Korea}

15 [\*]{now at: Korea Polar Research Institute, Incheon, Korea}

16 Correspondence to: J. Kim (jkim2@yonsei.ac.kr)

17  
18 **Abstract**

19 The performance of various empirical linear models to estimate the concentrations of surface-  
20 level particulate matter with a diameter less than 10  $\mu\text{m}$  (PM10) was evaluated using Aerosol  
21 Robotic Network (AERONET) sunphotometer and Moderate Resolution Imaging  
22 Spectroradiometer (MODIS) data collected in Seoul during the Distributed Regional Aerosol  
23 Gridded Observation Network (DRAGON)-Asia campaign from March to May 2012. An  
24 observed relationship between the PM10 concentration and the aerosol optical depth (AOD)  
25 was accounted for by several parameters in the empirical models, including boundary layer  
26 height (BLH), relative humidity (RH), and effective radius of the aerosol size distribution  
27 ( $R_{\text{eff}}$ ), which was used here for the first time in empirical modeling. Among various empirical  
28 models, the model which incorporates both BLH and  $R_{\text{eff}}$  showed the highest correlation,

1 which indicates the strong influence of BLH and  $R_{\text{eff}}$  on the PM<sub>10</sub> estimations. Meanwhile,  
2 the effect of RH on the relationship between AOD and PM<sub>10</sub> was appeared to be negligible  
3 during the campaign period (spring) when RH is generally low in Northeast Asia. A large  
4 spatial dependency of the empirical model performance was found by categorizing the  
5 locations of the collected data into three different site types, which varied in terms of the  
6 distances between instruments and source locations. When both AERONET and MODIS  
7 datasets were used in the PM<sub>10</sub> estimation, the highest correlations between measured and  
8 estimated values ( $R=0.76$  and  $0.76$  using AERONET and MODIS data, respectively) were  
9 found for the residential area (RA) site type, while the poorest correlations ( $R = 0.61$  and  $0.68$   
10 using AERONET and MODIS data, respectively) were found for the near source (NS) site  
11 type. Significant seasonal variations of empirical model performances for PM<sub>10</sub> estimation  
12 were found using the data collected at Yonsei University (one of the DRAGON campaign  
13 sites) over a period of 17 months including the DRAGON campaign period. The best  
14 correlation between measured and estimated PM<sub>10</sub> concentrations ( $R = 0.81$ ) was found in  
15 winter, due to the presence of a stagnant air mass and low BLH conditions, which may have  
16 resulted in relatively homogeneous aerosol properties within the BLH. On the other hand, the  
17 poorest correlation between measured and estimated PM<sub>10</sub> concentrations ( $R = 0.54$ ) was  
18 found in spring, due to the influence of the long-range transport of dust to both within and  
19 above the BLH.

20

## 21 **1 Introduction**

22 Atmospheric aerosols are known to play an important role in not only air quality but also  
23 climate change (Kaufman et al., 2002; WHO, 2005; IPCC, 2013). In terms of air quality,  
24 surface-level aerosol concentrations have been found to be strongly associated with impaired  
25 visibility (Baumer et al., 2008) and adverse effects on human health, such as respiratory and  
26 cardiovascular diseases (Pope et al., 2002; Kappos et al., 2004; Brook et al., 2010; Brauer et  
27 al, 2012). Therefore, several ground-based aerosol monitoring networks, such as the  
28 Interagency Monitoring of Protected Visual Environments (IMPROVE;  
29 <http://vista.cira.colostate.edu/improve/>), and the EPA's State and Local Air Monitoring  
30 Stations (SLAMS; <http://www.epa.gov/ttn/amtic/slams.html>), have been installed and  
31 operated to further understand the spatial and temporal variability of the chemical and  
32 physical characteristics of aerosols (Wang and Christopher, 2003).

1 However, due to the spatial limitations of in-situ measurements, the coordination of dense  
2 networks of multiple sites is required to monitor spatial variations in surface air quality in  
3 certain areas. To overcome the spatial limitations of such in-situ measurements, additional  
4 efforts have been made to estimate surface air quality from satellite measurements. Table 1  
5 summarizes the implementation of several different approaches that have been used to derive  
6 surface particulate matter (PM) concentrations using aerosol optical depth (AOD)  
7 measurements obtained from sunphotometer and satellite instruments. An empirical linear  
8 model using only AOD as a predictor for PM estimation showed correlation coefficients  
9 between measured and predicted PM<sub>2.5</sub> of 0.2-0.75 (Chu et al., 2003; Wang and Christopher,  
10 2003; Engel-Cox et al., 2004; Gupta and Christopher, 2008; Schaap et al., 2009). When the  
11 additional effects of boundary layer height (BLH) and relative humidity (RH) were  
12 incorporated into the empirical linear model (Engel-Cox et al., 2006; Koelemeijer et al., 2006;  
13 Emili et al., 2010; Wang et al., 2010), correlations between measured and predicted PM<sub>2.5</sub>  
14 were further improved when compared with correlations obtained from linear models using  
15 only AOD. A multiple linear regression model between measured and predicted PM<sub>2.5</sub>  
16 concentrations in urban areas yielded a correlation of 0.71 (Liu et al., 2007). Spatial  
17 distributions of PM<sub>2.5</sub> can also be estimated by applying the ratio of AOD to PM<sub>2.5</sub>, as  
18 calculated from chemical transport models (CTM), such as the Goddard Earth Observing  
19 System-Chemistry (GEOS-CHEM) transport model and the Community Multiscale Air  
20 Quality (CMAQ) model (Liu et al., 2004; Choi et al., 2009; van Donkelaar et al., 2010).  
21 These previous studies have demonstrated the strong possibility of deriving surface PM  
22 concentrations from AOD data.

23 However, if we are to further improve and validate PM estimates, additional physical  
24 parameters should be considered as inputs into the empirical models, so as to obtain accurate  
25 estimates of PM concentrations from AOD data. Additionally, the effects of various  
26 environmental characteristics on the relationship between PM and AOD, as well as spatial and  
27 temporal variations in this relationship, need to be investigated, especially in complex urban  
28 regions which include aerosol particles generated from various industrial and residential  
29 sources. Despite the need to monitor the rapidly changing PM concentrations in megacities  
30 with large populations and many sources of pollution, only a small number of studies have  
31 been conducted, especially in Asia, and the numbers of ground-based PM monitoring stations  
32 in these studies has been limited (Kumar et al., 2007; Guo et al., 2009). In addition to  
33 limitations based on sample size, obtaining accurate estimates of PM from AOD data has

1 proved difficult in Asia on account of the complexity of the aerosol compositions derived  
2 from both natural and anthropogenic sources, particularly during the spring (Kim et al., 2007;  
3 Song et al. (2009); Lee et al., 2010).

4 In an effort to address these problems, the present study uses aerosol measurements collected  
5 during the Distributed Regional Aerosol Gridded Observation Network (DRAGON)-Asia  
6 2012 campaign, which is just one of the DRAGON campaigns that has been conducted  
7 globally ([http://aeronet.gsfc.nasa.gov/new\\_web/DRAGON-  
8 Asia\\_2012\\_Japan\\_South\\_Korea.html](http://aeronet.gsfc.nasa.gov/new_web/DRAGON-Asia_2012_Japan_South_Korea.html)). The intensive DRAGON campaigns have provided  
9 valuable datasets, with well-coordinated measurements made in areas where aerosol  
10 concentrations are highly variable in space and time, and dependent on sources and other  
11 factors. The DRAGON campaigns have been conducted in urban and industrial areas,  
12 including Washington D.C., San Joaquin Valley of California, and Houston metropolitan  
13 region of Texas. By using the campaign datasets obtained from the dense coverage of both  
14 column and surface-level aerosol measurements, assessments of surface-level PM  
15 concentrations based on remote sensing observations can be substantially improved,  
16 especially in spring.

17 The purpose of this study is to investigate the relationship between AOD and PM  
18 concentrations in Seoul, one of the largest megacities in northeast Asia, using the DRAGON-  
19 Asia campaign dataset. The detailed objectives of this study are: (1) to estimate PM10  
20 concentrations using AOD data from both ground- and satellite-based measurements in a  
21 megacity, with additional consideration of the various parameters within the empirical  
22 models, and to thereby evaluate derived PM concentrations; (2) to identify the spatial  
23 variability of the empirical model performance at different types of measurement site; and (3)  
24 to investigate the seasonal variability of the performance of each model. Based on this study,  
25 it is expected that PM10 estimations using ground-based and satellite-derived AOD data will  
26 become an effective approach to monitoring air quality over large spatial domains, especially  
27 in complex urban areas.

28

## 29 **2 Measurements during the DRAGON-Asia campaign**

30 The study area, Seoul, is a megacity located in a downwind region of northeast Asia, in which  
31 air quality is often affected by both pollutants transported over long distances from  
32 continental interior and locally generated aerosol. The present study used the column aerosol

1 optical properties measured at 10 Aerosol Robotic Network (AERONET) sites in Seoul, as  
2 well as those obtained by a dense mesoscale network of ground-based instruments during the  
3 DRAGON-Asia 2012 campaign, which was conducted over the three-month period March–  
4 May 2012 (Fig. 1). The hourly-averaged PM<sub>10</sub> concentrations were also measured at 10 sites  
5 operated by a national air quality monitoring network during the campaign  
6 (<http://www.airkorea.or.kr>).

## 7 **2.1 Column AOD and surface PM measurements**

8 The AERONET sunphotometers (<http://aeronet.gsfc.nasa.gov/index.html>), which provide  
9 aerosol optical and microphysical properties based on direct sun and diffuse sky  
10 measurements (Holben et al., 1998), have been widely used as references for measurements  
11 from different satellite platforms. The AOD and the Angstrom exponent (AE) can be retrieved  
12 from direct sun measurements in several spectral bands, usually between 340 and 1020 nm  
13 (Holben et al., 1998). Diffuse sky measurements, which are performed at a minimum of four  
14 wavelengths (440, 670, 870, and 1020 nm), use an inversion method to provide detailed  
15 aerosol properties, such as the size distribution, phase function, single scattering albedo,  
16 refractive index, etc. (Holben et al., 1998; Dubovik and King, 2000). The AOD at 550 nm was  
17 obtained from AERONET level 2.0 direct sun measurements (cloud-screened and quality  
18 assured) at seven sites, and level 1.5 products (cloud-screened) at three sites. In addition to the  
19 AERONET AOD, the effective radius for the total (fine and coarse modes) size distribution  
20 obtained from the inversion product was also used to represent the aerosol size information in  
21 the empirical regression models (Dubovik and King, 2000). Although cloud-screened  
22 AERONET data were used, additional cloud screening was performed for further quality  
23 control using the cloud amount data provided by the Korea Meteorological Administration  
24 (KMA; <http://www.kma.go.kr>) and the attenuated backscattering signal measured from the  
25 two-wavelength Mie lidar located at Seoul National University (SNU). A cloud-free sky  
26 condition was defined as a cloud amount of less than 20% (cf. Ogunjobi et al., 2004) and no  
27 detections of strong scattering peaks of lidar measurements due to clouds. AOD  
28 measurements from the Moderate Resolution Imaging Spectroradiometer (MODIS) on board  
29 the Terra and Aqua satellites were also used to formulate the empirical regression models  
30 (Remer et al., 2005; Levy et al., 2007). To identify the optimal grid size for the MODIS AOD  
31 in this mesoscale spatial domain, the collocation criteria of the MODIS 550 nm AOD  
32 products collected at spatial resolutions of 10 and 30 km were tested and compared with

1 averaged AERONET 550 nm AOD measurements within  $\pm 30$  minutes of the satellite  
2 overpassing time. As shown in Figure 2, the MODIS and AERONET AOD data are highly  
3 correlated, showing a correlation coefficient (R) greater than 0.85 at most AERONET sites  
4 during the DRAGON-Asia campaign. At all AERONET sites except the DRAGON\_NIER  
5 station, higher correlations between AERONET and MODIS data were found for MODIS  
6 resolutions of 10 km than for those with MODIS resolutions of 30 km.

7 The MODIS AOD data at a 10 km resolution at nadir ('Optical\_Depth\_Land\_And\_Ocean')  
8 obtained from MODIS collection 5 aerosol products were also screened out when the MODIS  
9 cloud fraction over land ('Cloud\_Fraction\_Land') was higher than 0.5 or the cloud amount  
10 from the KMA was higher than 20%. Table 2 shows a statistical summary of the AERONET  
11 and MODIS AOD data that were available at the measurement sites for the entire campaign  
12 period before and after additional cloud screening. The maximum AERONET AOD was  
13 reduced by 1.57 (from 2.99 to 1.42) after additional cloud screening, while that of MODIS did  
14 not change. The mean and median AERONET AOD values were also reduced after cloud  
15 screening, and those of MODIS changed slightly. Also, the number of datasets after cloud  
16 screening was reduced by approximately 38.0%, and the reduction in the available MODIS  
17 data after cloud screening was 13.7%.

18 Hourly averaged PM<sub>10</sub> concentrations, measured routinely at 10 national air quality  
19 monitoring sites, were used during the DRAGON-Asia campaign. The PM<sub>10</sub> concentrations  
20 were measured by a beta ( $\beta$ )-ray absorption method using a PM<sub>10</sub> Beta Gauge (model  
21 PM10B.G, W&A Inc.), which operates on the premise that the absorption of beta-rays  
22 increases in proportion to the number of particles collected in the filter (Hauck et al., 2004).

23 To investigate the relationship between columnar AOD and surface-level PM<sub>10</sub>, the  
24 measurements must be collocated both spatially and temporally. The AERONET AOD data  
25 obtained from the station nearest to the PM monitoring site (within a maximum distance of  
26 approximately 4.5 km) were used. On the other hand, the MODIS AOD data, which were  
27 measured at different spatial grid resolutions, were extracted within a maximum distance of  
28 0.2° of the PM<sub>10</sub> measurement sites. The AERONET and MODIS AOD were both  
29 temporally collocated within  $\pm 30$  minutes of the hourly PM<sub>10</sub> measurement time.

## 1 2.2 Meteorological measurements

2 Meteorological data were used to investigate the relationship between AOD and PM10  
3 concentrations. The attenuated backscatter coefficient at 532 nm, measured by the two-  
4 wavelength Mie lidar located at Seoul National University ([http://www-  
5 lidar.nies.go.jp/Seoul/](http://www-lidar.nies.go.jp/Seoul/)), was used to calculate the hourly BLH using the automated wavelet  
6 covariance transform (WCT) method (Brooks, 2003). The WCT method was applied to  
7 backscattered lidar signals at heights above 300 m from the surface to avoid the problem of  
8 uncertainty in lidar overlap (Campbell et al., 2002). Figure 3 shows an example of temporal  
9 variation in the BLH obtained by application of the WCT method.

10 In addition to the BLH, other meteorological data such as temperature, relative humidity,  
11 cloud amount, and wind speed and direction were obtained from hourly measurements at a  
12 KMA weather observation station in Seoul (37.57°N, 126.97°E). All meteorological data  
13 within  $\pm 30$  min of the PM10 observation time were used for this investigation.

14

## 15 3 Methodology

### 16 3.1 Relationship between column AOD and surface PM concentration

17 The AOD is the integration of the radiative extinction due to aerosols from the surface up to  
18 the top of the atmosphere (TOA) at a given wavelength. The AOD can be defined as  
19 (Koelemeijer et al., 2006):

$$\begin{aligned} AOD &= \pi \int_0^H \int_0^\infty Q_{ext,amb}(m, r, \lambda) n_{amb}(r, z) r^2 dr dz \\ &= \pi f(RH) \int_0^H \int_0^\infty Q_{ext}(m, r, \lambda) n(r, z) r^2 dr dz, \end{aligned} \quad (1)$$

21 where  $Q_{ext,amb}(m, r, \lambda)$  is the unitless extinction efficiency influenced by the refractive index  
22 ( $m$ ), particle radius ( $r$ ), and wavelength ( $\lambda$ ) under ambient conditions,  $Q_{ext}(m, r, \lambda)$  the  
23 extinction efficiency under dry conditions,  $n_{amb}(r, z)$  the size distribution under ambient  
24 conditions representing the number of aerosols at corresponding height ( $z$ ) with a radius ( $r$ ),  
25  $n(r, z)$  the size distribution under dry conditions and  $H$  the top height for the integration.

1 The PM10 concentration, which is the mass concentration of surface-level aerosols with  
 2 diameters less than 10  $\mu\text{m}$  in dry conditions, is given by:

$$3 \quad PM_{10} = \frac{4}{3} \pi \rho \int_0^5 r^3 n(r) dr \quad (2)$$

4 where  $\rho$  is the particle mass density and  $r$  is the dry aerosol radius. With the assumption of a  
 5 homogeneous aerosol distribution within the BLH, the integration from the surface up to the  
 6 TOA ( $H$ ) can be simplified by multiplying by the BLH. Also, the ambient environmental  
 7 condition can be converted into the dry condition by using the particle hygroscopic growth  
 8 factor,  $f(\text{RH})$ . By combining Eqs (1) and (2), the PM10 concentration can be expressed as:

$$9 \quad PM_{10} = \frac{AOD}{BLH \cdot f(\text{RH})} \frac{4\rho R_{\text{eff}}}{3\langle Q_{\text{ext}} \rangle} \quad (3)$$

10 where the effective radius  $R_{\text{eff}}$  and the average of the extinction efficiency over the size  
 11 distribution  $\langle Q_{\text{ext}} \rangle$  are defined as

$$12 \quad R_{\text{eff}} = \frac{\int r^3 n(r) dr}{\int r^2 n(r) dr}, \quad \langle Q_{\text{ext}} \rangle = \frac{\int r^2 Q_{\text{ext}}(r) n(r) dr}{\int r^2 n(r) dr}.$$

13 In order to extend this analysis to the PM2.5, upper size limit in integral in Eq.(2) need to be  
 14 corrected and fine mode fraction (FMF) to be additionally considered in Eq.(3). However,  
 15 since available PM2.5 measurements were quite limited in this area and time, we focused only  
 16 PM10 in this present study. In Eq. (3), various physical parameters are involved in the  
 17 relationship between AOD and PM10. The PM10 concentration is proportional to AOD,  $R_{\text{eff}}$ ,  
 18 and particle mass density  $\rho$ ; on the other hand, PM10 is inversely proportional to BLH,  $f(\text{RH})$ ,  
 19 and  $\langle Q_{\text{ext}} \rangle$ . To gain insights of the relationship between PM10 and major predictors, all  
 20 PM10 concentration was plotted against AOD, BLH, RH, and  $R_{\text{eff}}$ , which were used in this  
 21 study for development and validation of PM10 estimation as shown in Fig 4. The correlation  
 22 coefficient (R) between PM10 and AOD was 0.5 and that of  $R_{\text{eff}}$  was 0.32. As expected, BLH  
 23 showed negative correlation with PM10 (-0.36). However, RH did not show any significant  
 24 relationship with PM10. Among these parameters, BLH and  $f(\text{RH})$  have been used as  
 25 parameters in empirical models to estimate PM concentrations using AOD data, as described  
 26 in Table 1. On the other hand, parameters such as  $\rho$ ,  $R_{\text{eff}}$ , and  $\langle Q_{\text{ext}} \rangle$  have been rarely included  
 27 in empirical models. In the present study, the effective radius of the aerosol size distribution



1 was included for the first time as an additional parameter in the empirical models. The  
2 empirical models, and the parameters considered in those models, are described in detail in  
3 Section 3.2.

### 4 **3.2 Description of empirical linear models for PM10 estimation**

5 Table 3 presents a summary of the various models used in this study. Models M1 to M5 are  
6 empirical models based on the relationship between AOD and PM concentration, as described  
7 in Section 3.1, whereas M6 represents a multiple linear regression model. Among the  
8 empirical models, M1, M2, and M4 have been used in previous studies (e.g., Chu et al., 2003;  
9 Wang and Christopher, 2003; Engel-Cox et al., 2004, 2006; Koelemeijer et al., 2006; Gupta  
10 and Christopher, 2008; Schaap et al., 2009; Emili et al., 2010; Wang et al., 2010). Model M1  
11 includes only AOD as a predictor of the PM10 concentration, while M2 additionally includes  
12 BLH to consider the aerosol vertical extension. The vertical correction on AOD is represented  
13 in M2 by dividing AOD by BLH, with the assumption that aerosols within the boundary layer  
14 are homogeneously mixed. Model M4 corrects for RH by using an aerosol hygroscopic  
15 growth factor term  $f(\text{RH})$  which represents the effects of aerosol hygroscopic growth caused  
16 by variations in relative humidity, in addition to the parameters in M2. In this study,  $f(\text{RH})$   
17 based on experimental data obtained near the Beijing mega-city during the spring was  
18 employed (Pan et al., 2009), which is appropriate to this study with respect to both temporal  
19 and spatial conditions. Models M3 and M5, which also included the parameters used in M1,  
20 M2, and M4, were the first empirical models to include the effective radius of the aerosol size  
21 distribution as a size correction factor. Model M3 includes the aerosol effective radius in  
22 addition to the parameters in M2 to account for the size of aerosol particles. Model M5  
23 reflects all parameters, including AOD,  $f(\text{RH})$ , BLH, and the effective radius, as shown in  
24 Table 3. The effective radius of the aerosol size distribution for the total mode, which was  
25 used in M3 and M5, was obtained from AERONET inversion products (Dubovik and King,  
26 2000; Dubovik et al., 2000). This  $R_{\text{eff}}$  is one of the main features derived by the particle  
27 volume size distribution retrieved by AERONET inversion algorithm, which was  
28 demonstrated to be adequate in practically all situations, especially, for the intermediate  
29 particle size range ( $0.1 \leq r \leq 7 \mu\text{m}$ ) with 10-35% of retrieval errors, as reported by Dubovik et  
30 al. (2002).

31 In addition to the simple empirical models (M1-M5) derived from the relationship between  
32 AOD and PM (Eq. (3)), a multiple linear regression (MLR) model was used as a statistical

1 approach to determine PM10 concentrations as a function of eight different parameters  
2 associated with PM estimation:

$$3 \quad [PM_{10}] = \exp(\beta_0) \times (AOD)^{\beta_{AOD}} (BLH)^{\beta_{BLH}} (AE)^{\beta_{AE}} \times \exp[\beta_{loc}(Location) + \beta_{WS}(WS) + \beta_{WD}(WD) + \beta_{RH}(RH) + \beta_{Temp}(Temp)]$$

4 (4)

5 This MLR model of Eq. (4) can be log-transformed into a simpler form of linear regression as  
6 shown in Eq. (5).

$$7 \quad \ln[PM_{10}] = \beta_0 + \beta_{AOD} \ln(AOD) + \beta_{BLH} \ln(BLH) + \beta_{AE} \ln(AE) + \beta_{loc}(Location) + \beta_{WS}(WS) + \beta_{WD}(WD) + \beta_{RH}(RH) + \beta_{Temp}(Temp)$$

8 (5)

9 The dependent variable in Eq. (5) is the logarithm of the hourly PM10 concentration  
10 measured at the PM monitoring sites. The independent variables include aerosol optical  
11 properties such as AOD and AE, various meteorological measurements such as BLH,  
12 temperature (Temp), and wind speed (WS), and two categorical variables: type of  
13 measurement site (Location) and wind direction (WD). The  $R_{eff}$  inversion product is from  
14 diffuse sky radiance measurement which has strict stability criteria. Thus, the number of data  
15 (N=713) is quite lower than products from direct sun measurements including AE (N=2112)  
16 which also implies the aerosol size information. For that reason, AE was used as a variable in  
17 the MLR model instead of  $R_{eff}$  to secure enough number of data sample (Dubovik et al., 2000;  
18 Schuster et al., 2006). Measurement sites were categorized into three types: near source (NS),  
19 typical urban (TU), and residential area (RA), as shown in Fig. 1. The NS sites were those  
20 located within 500 m of sources; sources in this case included traffic-congested roads and  
21 industrial complexes. The TU sites were located more than 500 m from sources, in either  
22 commercial or residential areas. The RA sites were located more than 500 m from sources and  
23 in residential areas only. Wind directions were classified as east, south, west, or north.  
24 Regression coefficients ( $\beta$ ) were determined for each of the independent variables. This MLR  
25 analysis was conducted using AERONET dataset only, because this was sufficient to yield  
26 credible results.

27 For an unbiased assessment of model performance, the entire AERONET dataset was  
28 randomly divided into two groups, a modeling group (N = 1058 for M1, M2, M4, and M6,  
29 and N = 369 for M3 and M5) that was used to develop the empirical models, and a validation  
30 group (N = 1054 for M1, M2, M4, and M6, and N = 373 for M3 and M5) that was used to  
31 validate these models. To minimize the effects of temporal autocorrelation, data were selected

1 such that the time interval between validation and modeling data was at least 24 h. Summary  
2 statistics for the variables involved in the modeling and validation datasets are shown in Fig. 5.  
3 All empirical models for hourly PM10 estimates based on the AERONET datasets were fitted  
4 using the modeling dataset to estimate the model coefficients. Estimated regression  
5 coefficients ( $\beta$ ), standard errors, and  $p$ -values of parameters used in M6 (Eq. (5)) are  
6 summarized in Table 4. As shown in Table 4, most parameters used in M6 were found to be  
7 highly significant ( $p < 0.0001$ ) predictors of the PM10 concentration. The positive sign of the  
8 coefficient for AOD ( $0.527 \pm 0.022$ ) shows a direct correspondence between AOD and  
9 surface PM10, given that other conditions remained constant. On the other hand, the  
10 estimated power of the BLH relationship was negative ( $-0.280 \pm 0.028$ ), which indicates an  
11 inverse relationship between BLH and the PM10 concentration. The reason for this inverse  
12 relationship is that a lower BLH confines aerosols to a thinner atmospheric layer, resulting in  
13 higher surface PM10 concentrations. A negative coefficient was also obtained for RH ( $-0.610$   
14  $\pm 0.116$ ), showing that higher RH conditions result in lower PM10 concentrations (given  
15 constant AOD values); i.e., the effect of aerosol hygroscopic growth is reflected in the MLR  
16 model (M6).

17 In this analysis, MODIS datasets collected over Seoul during the DRAGON-Asia campaign  
18 were not divided into two groups (for model development and validation) due to the relatively  
19 small size of the MODIS dataset obtained during the campaign ( $N = 252$  for M2 and M4; as  
20 compared with  $N = 1054$  for M2 and M4 for the AERONET dataset).

21

## 22 **4 Results and discussion**

### 23 **4.1 Evaluation of estimated PM10 using various empirical linear models**

24 The hourly PM10 concentrations estimated by the various empirical models were evaluated  
25 by comparing them with measured hourly surface-level PM10. Table 5 shows a summary of  
26 the correlations and statistics between the measured and estimated PM10 concentrations using  
27 the various model types, obtained using the AERONET and MODIS datasets. The simplest  
28 model (M1), with only AOD as a predictor, yields the lowest correlation of 0.40 (0.46) using  
29 the AERONET (MODIS) dataset for the PM10 estimation. The correlation obtained using the  
30 cloud-screened AOD data (M1<sub>c</sub>) is higher than that obtained using the raw AOD data (M1),  
31 which implies that cloud screening contributes to an increase in the correlation between

1 measured PM and AOD by removing overestimated AOD measurements resulting from cloud  
2 contamination (e.g. Schaap et al., 2009).

3 Model M2, in which BLH is an added parameter, shows a correlation coefficient of 0.62 (0.72)  
4 and a root mean square error (RMSE) of 22.11 (23.02)  $\mu\text{g}/\text{m}^3$  between measured and  
5 estimated PM10 using the AERONET (MODIS) AOD data; in this case, the estimate using  
6 MODIS AOD data as an input is a better predictor than the estimate obtained using the  
7 AERONET data (Table 5). This higher performance of the MODIS AOD and model M2 can  
8 be attributed to a MODIS overpass time near midday, when aerosols are generally well mixed  
9 in the boundary layer, as compared with the situation in the early morning or late afternoon.  
10 These improved correlation coefficients imply that a vertical correction on AOD using the  
11 BLH value improves PM10 estimates. The correlations between measured and estimated  
12 PM10 using M2 with MODIS data are slightly higher than those obtained in the previous  
13 work of Emili et al. (2010), which was based on a combination of Spinning Enhanced Visible  
14 and Infrared Imager (SEVIRI) and MODIS AOD data to estimate hourly PM10  
15 concentrations over the European Alpine regions. The differences between the results of  
16 Emili et al. (2010) and those obtained here could be associated with uncertainties in surface  
17 reflectance in alpine regions that resulted in relatively larger errors in the alpine AOD data as  
18 compared with those obtained in Seoul.

19 Aerosol effective radius data obtained from AERONET measurements was used as a  
20 parameter in model M3 to estimate PM10. The effective radius of aerosol, as derived from  
21 sky radiances obtained from solar almucantar measurements, is available only when the solar  
22 zenith angle (SZA) is larger than  $50^\circ$  (except for near local noon), which avoids polarization  
23 effects (Holben et al., 1998; Dubovik and King, 2000). Consequently, in contrast to the AOD  
24 data, the effective radius data is available only in a limited time window. The limited number  
25 of effective radius measurements was used as an input to M3 to estimate PM10; we used 35.4%  
26 ( $N = 373$ ) of the total number of AERONET validation datasets ( $N = 1054$ ) in which data  
27 were simultaneously available for both AOD and the effective radius. Model M3 was not  
28 implemented using MODIS AOD due to a lack of effective radius information in the MODIS  
29 datasets over land areas. As shown in Table 5, the correlation between measured PM10 and  
30 those estimated from M3 is higher than that obtained using M2 with the same number of  
31 datasets ( $N = 373$ ;  $R_{M3,AERO} = 0.55$ ,  $R_{M2,AERO} = 0.46$ ). Although the results are subject to  
32 further validation, aerosol size corrections using the effective radius (M3), in general, lead to

1 better estimates of PM10 concentrations than do those without (M2), at least during the time  
2 frame of the intensive campaign period.

3 Model M4, which incorporates the aerosol hygroscopic growth factor ( $f(\text{RH})$ ) in PM10  
4 estimation, yields a correlation coefficient of 0.63 (0.71) for the AERONET (MODIS) dataset  
5 (Table 5). These correlations are similar to those obtained using M2, in which the RH  
6 correction is absent. The results suggest that RH levels do not significantly influence BLH-  
7 corrected estimates at our measurement sites during the campaign period, during which  
8 average daytime RH values were  $30.5\% \pm 11.0\%$ ; at these RH levels, it appears that aerosols  
9 are largely unaffected by hygroscopic growth.

10 The PM10 estimates derived from M5, which considers BLH,  $f(\text{RH})$ , and the effective radius,  
11 were also evaluated by comparisons with PM10 concentrations measured at the surface. As  
12 discussed previously, the number of samples for the effective radius used in M3 ( $N = 373$ )  
13 was also used in M5, and M5 was also evaluated using the AERONET data. Table 5 shows  
14 that the correlation coefficient obtained using model M5 was 0.58, while those from M3 and  
15 M4 were 0.55 and 0.47, respectively, using the same number of datasets ( $N = 373$ ). The  
16 correlation between measured and estimated PM10 concentrations obtained from M5 is  
17 higher than that obtained from M4, on account of the addition of aerosol size information.  
18 However, this correlation obtained from M5 is slightly improved relative to that obtained  
19 from M3, as the effect of the RH correction is considered to be negligible for PM10  
20 estimations using data collected during the DRAGON-Asia campaign when average RH  
21 values were low.

22 The PM10 concentrations were also estimated from the MLR model (M6). As discussed in  
23 Section 3.2, 1054 AERONET datasets were used for the validation of PM10 estimated using  
24 M6. The correlation coefficient between the measured PM10 and those estimated from M6 is  
25 0.68. This correlation coefficient is the highest among those obtained by any of the empirical  
26 models in this study, and shows that various meteorological parameters, such as RH,  
27 temperature, wind speed, and wind direction, contribute to a substantial increase in the  
28 accuracy of PM10 estimates.

29 The BLH and the effective radius of aerosols are the dominant predictors of PM10 in the  
30 empirical models, while the effect of RH on PM10 estimation during the campaign period is  
31 negligible. However, the contribution of the RH correction may vary seasonally, which is  
32 further discussed in Section 4.3. In terms of the errors in the estimated PM10 concentrations,

1 the RMSE of PM10 estimated using M6 (M2) with the input of the AERONET (MODIS)  
2 dataset is 21.05 (23.02)  $\mu\text{g}/\text{m}^3$ , which is the lowest among those calculated with the empirical  
3 models (Table 5). The RMSE values between measured PM10 concentrations and those  
4 estimated using M1<sub>cl</sub> (N = 1054), M2 (N = 1054), and M4 (N = 1054), based on the same  
5 number of AERONET datasets as inputs, are 23.79, 22.11, and 22.11  $\mu\text{g}/\text{m}^3$ , respectively,  
6 showing that the models tend to improve (i.e., the errors tend to decrease) when using the  
7 BLH as a predictor in the empirical models. This improvement in the models was also found  
8 when a vertical correction is applied to the MODIS data. The RMSE values of PM10  
9 estimated using M1<sub>cl</sub> (N = 252), M2 (N = 252), and M4 (N = 252), and based on inputs of  
10 MODIS data, were 28.55, 23.02, and 23.19  $\mu\text{g}/\text{m}^3$ , respectively. The RMSE values of PM10  
11 estimated using M2 (N = 373), M3 (N = 373), and M5 (N = 373), and based on the same  
12 number of AERONET datasets, were 23.27, 22.01, and 21.32  $\mu\text{g}/\text{m}^3$ , respectively, when a size  
13 correction using the aerosol effective radius and an RH correction using the particle  
14 hygroscopic growth factor were incorporated into the models. To evaluate the empirical  
15 model performance for PM10 estimation, the mean normalized bias (MNB) and the mean  
16 fractionalized bias (MFB) were also calculated (these statistical parameters are described in  
17 the footnote of Table 5). The tendencies of both the MNB and MFB are similar to those of the  
18 RMSE, except for M6. All MFB values (except for M6) are positive, which indicates that the  
19 PM10 concentrations derived from the models are generally overestimated when compared  
20 with measured PM10 values. The MFB of M6 was  $-0.83\%$ , which shows that M6 tends to  
21 underestimate the PM10 concentration, especially at high concentrations on account of the log  
22 transformation of the data.

## 23 **4.2 Spatial characteristics of correlations between measured and estimated** 24 **PM10**

25 Large variations in the mean and standard deviation of the measured PM10 concentrations  
26 were observed, with the size of the deviations dependent on the measurement site type. As  
27 described in Section 3.2, the site types include near source (NS), typical urban (TU), and  
28 residential area (RA) site types in Seoul, as identified during the DRAGON-Asia campaign.  
29 The means (standard deviations) of the hourly measured PM10 concentration in Seoul during  
30 the campaign period were 62.21 ( $\pm 33.78$ ), 53.42 ( $\pm 28.40$ ), and 52.19 ( $\pm 26.15$ )  $\mu\text{g}/\text{m}^3$  at the  
31 NS, TU, and RA site types, respectively. The highest mean and standard deviation of the

1 PM10 concentrations were found at the NS site type, while the lowest were found at the RA  
2 site type.

3 To identify spatial variability within the performance of the empirical models, the correlations  
4 between measured and estimated PM10 concentrations were further investigated with respect  
5 to the classification of site types (NS, TU, and RA). Table 6 shows the correlations between  
6 measured and estimated PM10, with inputs of AERONET and MODIS data, and as dependent  
7 on the measurement site type. As shown in Table 6, correlation coefficients for the RA site  
8 show good model performances (0.69–0.76) using M3, M5, and M6; however, model  
9 performances for the NS and TU site types fall within the ranges 0.59–0.61 and 0.61–0.72,  
10 respectively. Correlation coefficients for the RA site type are in the range 0.63–0.73 for  
11 models M1<sub>cl</sub>, M2, and M4, whereas those for the NS and TU site types are 0.49–0.57 and  
12 0.51–0.61, respectively. The RMSE values are 16.53–19.67, 17.69–22.61, and 22.85–26.79  
13  $\mu\text{g}/\text{m}^3$  for the RA, TU, and NS site types, respectively, showing that errors in PM10 estimates  
14 at NS site types are higher than those at TU and RA site types. Thus, the highest correlation in  
15 each empirical model was obtained for the RA sites, while the lowest was found at the NS  
16 sites (Table 6). The NS site type shows large spatial and temporal variability in surface PM10  
17 concentrations due to large anthropogenic aerosol emissions, which presents difficulties in the  
18 development of empirical models for estimating PM10 concentrations. The results obtained  
19 using the AERONET data (Table 6) also demonstrate that hourly PM10 estimations depend  
20 largely on both the empirical model used for the estimation and the site type in megacity areas,  
21 where the spatial and temporal variability of aerosol concentrations is large.

22 As discussed in Section 4.1, the spatial dependency of empirical model performance using the  
23 MODIS data inputs was investigated only for models M1<sub>cl</sub>, M2, and M4, due to a lack of  
24 effective radius information in the MODIS data. The spatial dependency of the empirical  
25 model performance using the MODIS data is large. Table 6 shows the highest correlations for  
26 the RA site type, while the lowest are for the NS sites. The correlation coefficients for the RA  
27 sites were between 0.50 and 0.76 for models M1<sub>cl</sub>, M2, and M4, whereas those for the TU and  
28 NS sites were 0.42–0.72 and 0.37–0.68, respectively. The highest correlation between  
29 measured and estimated PM10, obtained using M2 with MODIS data, was comparable with  
30 those obtained using M5 and M6 with AERONET data. This high performance of the  
31 empirical models using the MODIS data can be explained by the overpass time of the MODIS

1 data, which was around midday when aerosols are generally well-mixed within the boundary  
2 layer compared with other times of the day (Schaap et al., 2009).

3 The inverse distance weighting (IDW) interpolation method was applied to estimate the PM10  
4 concentrations using M2 with MODIS AOD data over various campaign sites, at a spatial  
5 resolution that was finer than that established for the original MODIS data (10 km). The IDW  
6 method was used to estimate PM10 concentrations in alpine regions with simple PM source  
7 distributions (Emili et al., 2010). In this study, model M2 with MODIS AOD and lidar BLH  
8 data was used to estimate PM10 concentrations at a resolution of  $0.02^\circ$  (ca. 2 km) over the  
9 Seoul area. Slopes and intercepts of M2 were spatially interpolated to a resolution of  $0.02^\circ$   
10 using the IDW method, as calculated from values at the four closest pixels. Figure 6 shows  
11 PM10 estimates at the 2 km resolution based on the IDW method, where the colored circles  
12 represent PM10 concentrations measured at PM monitoring sites. The spatial distribution of  
13 the estimated and measured PM10 concentrations is generally in good agreement. However, a  
14 discontinuity is observed in Fig. 6, which could be due to a problem associated with AOD  
15 input at a low resolution and its interpolation based on inhomogeneous sampling of a small  
16 number of data points. In order to understand smaller scale features of the air quality, higher  
17 spatial resolution AOD products such as a MODIS 3km product are under development.  
18 Although this high resolution product has been expected to explain aerosol gradients in detail  
19 at a small scale, the 3km product showed poor performances compared to the 10 km product  
20 due to improper characterization of the urban surfaces (Levy et al., 2013; Munchak et al.,  
21 2013). This bias in surface reflectance of MODIS algorithm indeed resulted in misfit between  
22 column AOD and surface PM concentration, as discussed in Escribano et al. (2014). Thus,  
23 estimated spatial characteristics of surface PM concentrations are reliable when aerosol  
24 products are satisfied with both higher quality and finer resolution.

### 25 **4.3 Seasonal characteristics of correlations between measured and estimated** 26 **PM10**

27 The empirical models proposed in Section 3.2 were applied to data collected for an extended  
28 time period (beyond that of the DRAGON-Asia campaign) at a Yonsei University (YU) site  
29 to investigate the seasonal characteristics of the various empirical model performances for  
30 PM10 estimation. Seasonal effects were studied during all four seasons (spring, summer,  
31 autumn, and winter), defined here as the periods March–May, June–August, September–  
32 November, and December–February, respectively. The AERONET level 2.0 data were used



1 from March 2011 to July 2012 at the YU site, as YU is the only site in Seoul where  
2 AERONET level 2.0 data are available for the period that covers all four seasons, and which  
3 also includes the DRAGON-Asia campaign period. All models except for MLR model M6  
4 were used to identify the seasonal dependency of model performance; M6 was not used  
5 because the number of datasets was insufficient to determine the regression coefficients for  
6 the four different seasons.

7 Table 7 summarizes the seasonal variations in the correlations between measured and  
8 estimated PM10 using the various empirical models and the AERONET data. The overall  
9 statistics (including correlation coefficients) of the models using the AERONET data were  
10 found to be poorest in spring, when compared with those of other seasons. Correlation  
11 coefficients using all empirical models and the AERONET data (Table 7) were in the range  
12 0.39–0.54 for spring, whereas those for summer, autumn, and winter were 0.64–0.71, 0.52–  
13 0.66, and 0.63–0.81, respectively. The poor performance in spring can be attributed to  
14 frequent occurrences of Asian dust events as well as persistent anthropogenic influences at  
15 YU which is located in a continental downwind region. The Asian dust events in spring  
16 generate inhomogeneous aerosol vertical distributions due to elevated aerosol layers above  
17 the BLH, which are not taken into account by using BLH in the empirical models (Murayama  
18 et al., 2001; Kim, S. et al., 2007). Therefore, the performance using M2 in spring ( $R = 0.47$ ) is  
19 still much poorer than performances in other seasons ( $R \geq 0.64$ ), which could be attributed to  
20 the presence of multiple aerosol layers and mixtures of different types of aerosols in spring.

21 The highest correlations of estimated and measured PM10 concentrations occur in winter  
22 using M3 and M5 ( $R = 0.81$ ), which both consider the BLH and the effective radius of aerosol.  
23 In winter, a lower aerosol mixing height and homogeneous microphysical and optical  
24 properties within the BLH are thought to result in BLH and the effective radius being the  
25 dominant predictors in the empirical models for PM10 estimation. A lower aerosol mixing  
26 height is often induced by a temperature inversion in winter, when homogeneous aerosol  
27 properties are likely to be present within the boundary layer due to the reduced influence of  
28 the long-range transport of aerosols above the BLH. The correlation using M4, which  
29 considers BLH and RH in summer ( $N = 85$ ) and autumn ( $N = 212$ ), when RH is relatively  
30 higher than in the other two seasons, yields correlations of 0.71 and 0.66, respectively. In  
31 summer, the RH correction improves the PM10 estimation, yielding a correlation of 0.71  
32 using M4 compared with a correlation of 0.67 using M2. In autumn, incorporation of the RH

1 correction into the models (M4) yields a slightly improved correlation compared with models  
2 that exclude the RH correction (M2); i.e., 0.66 and 0.64, respectively. The correlation also  
3 increases from 0.64 (M3) to 0.66 (M5), and from 0.54 (M3) to 0.58 (M5), in summer and  
4 autumn, respectively, when including the RH correction, which shows that the RH correction  
5 is effective in conditions of higher RH.

6

## 7 **5 Conclusions**

8 Concentrations of PM<sub>10</sub> were estimated in Seoul, Korea during the DRAGON-Asia campaign  
9 period by considering the effective radius of the aerosol size distribution, together with BLH,  
10 RH, and AOD, within empirical models that used AERONET data obtained at multiple sites  
11 for the first time. The performances of various empirical models were also evaluated for  
12 hourly PM<sub>10</sub> estimations using AERONET and MODIS datasets. The improved  
13 performances were found when the vertical correction on AOD using the BLH was applied in  
14 both AERONET and MODIS datasets (M2) compared to the simplest model (M1). These  
15 empirical model performances were further enhanced by additionally including the effective  
16 radius for size correction (M3, M5). However, not meaningful improvements were found  
17 when RH was considered additionally (M4). Among different empirical models based on the  
18 physical relationship between AOD and PM concentration (M1-M5), model M5 which  
19 follows the nearest form of that relationship with the largest number of parameters showed the  
20 best performance. In general, BLH and the effective radius were found to be the key  
21 parameters when estimating PM<sub>10</sub> using the empirical models, while RH did not show any  
22 significant effect on PM<sub>10</sub> estimation using the multiple datasets collected during the spring  
23 campaign period, when RH is relatively lower than summer and autumn.

24 The spatial variability of empirical model performance was also investigated for three  
25 different site types, which were categorized according to the distance between sources and  
26 instruments. The highest correlation for each empirical model using both AERONET and  
27 MODIS data occurred for the RA sites, while the lowest was for the NS sites, where the  
28 spatio-temporal variability of aerosols is high. The selection of site types either dominates, or  
29 is comparable with, the specific empirical model selected for estimating PM<sub>10</sub> concentrations  
30 in Seoul, as results are significantly affected by the spatial variability of aerosols. The  
31 performances of the models for estimating PM<sub>10</sub> were also good at midday when aerosols are

1 well mixed within the boundary layer, which suggests a dependence of PM10 estimation on  
2 the measurement time.

3 Seasonal variations in the performances of the empirical models for PM10 estimation were  
4 detected. The highest correlation was found using M3 and M5 in winter ( $R = 0.81$ ), when  
5 both BLH and the effective radius of the aerosol are considered; the high correlations can be  
6 attributed to a lower aerosol mixing height and homogeneity in the optical and microphysical  
7 properties of aerosols within the BLH. The poorest performance was found in spring, when  
8 the impact of Asian dust events on both inhomogeneous vertical structure of particle number  
9 and aerosol composition at the measurement sites is common, and leads to variable effects.

10 As discussed in this study, the spatial distribution of surface-level PM10 concentrations can  
11 be estimated using empirical models. The use of satellite measurements in these various  
12 empirical models has the advantage of both simplicity and wide spatial coverage over  
13 megacity areas. However, the predictability of PM10 distributions using empirical models  
14 should be improved. For better estimating surface PM concentrations by satellite remote  
15 sensing, especially in urban areas where diverse aerosol sources are distributed, aerosol  
16 products with a higher quality and a finer resolution are required. Additionally, accurate and  
17 detailed information about aerosol vertical distribution, size distribution, and composition will  
18 contribute to improve empirical models. Also, to enhance the accuracy of PM10 estimations  
19 in other seasons, further work is required to investigate seasonal effects on the spatial  
20 variability of PM10 estimations in Seoul. In addition to the evaluation of multiple empirical  
21 models in the megacity area, a chemistry transport model (CTM) should also be performed  
22 and validated for PM10 estimations.

23

## 24 **Acknowledgements**

25 This research was supported by the GEMS program of the Ministry of Environment, Korea  
26 and the Eco Innovation Program of KEITI (2012000160002). The authors deeply appreciate  
27 NIER and the staff for the DRAGON-Asia campaign in establishing and maintaining the  
28 AERONET sites. We would also like to thank NIER for the PM10 data used, NASA for the  
29 AERONET and MODIS data, and NIES Lidar team for the lidar data. This research was  
30 partially supported by the Brain Korea 21 Plus for SS, JK, HL, WJ, and WK.

31

## 1 **References**

- 2 Baumer, D., Vogel, B., Versick, S., Rinke, R., Mohler, O., and Schnaiter, M.: Relationship of  
3 visibility, aerosol optical thickness and aerosol size distribution in an ageing air mass over  
4 South-West Germany, *Atmos. Environ.*, 42, 989-998, DOI 10.1016/j.atmosenv.2007.10.017,  
5 2008.
- 6 Brauer, M., Amann, M., Burnett, R. T., Cohen, A., Dentener, F., Ezzati, M., Henderson, S. B.,  
7 Krzyzanowski, M., Martin, R. V., and Van Dingenen, R.: Exposure assessment for estimation  
8 of the global burden of disease attributable to outdoor air pollution, *Environ. Sci. Technol.*, 46,  
9 652-660, 2012.
- 10 Brook, R. D., Rajagopalan, S., Pope, C. A., Brook, J. R., Bhatnagar, A., Diez-Roux, A. V.,  
11 Holguin, F., Hong, Y. L., Luepker, R. V., Mittleman, M. A., Peters, A., Siscovick, D., Smith,  
12 S. C., Whitsel, L., Kaufman, J. D., *Epidemiol. A. H. A. C.*, Dis, C. K. C., and *Metab.*, C. N. P.  
13 A.: Particulate Matter Air Pollution and Cardiovascular Disease An Update to the Scientific  
14 Statement From the American Heart Association, *Circulation*, 121, 2331-2378, 2010.
- 15 Brooks, I. M.: Finding boundary layer top: Application of a wavelet covariance transform to  
16 lidar backscatter profiles, *J. Atmos. Oceanic Tech.*, 20, 1092-1105, 2003.
- 17 Campbell, J. R., Hlavka, D. L., Welton, E. J., Flynn, C. J., Turner, D. D., Spinhirne, J. D.,  
18 Scott, V. S., and Hwang, I. H.: Full-time, eye-safe cloud and aerosol lidar observation at  
19 atmospheric radiation measurement program sites: Instruments and data processing, *J. Atmos.*  
20 *Oceanic Tech.*, 19, 431-442, 2002.
- 21 Choi, Y. S., Park, R. J., and Ho, C. H.: Estimates of ground-level aerosol mass concentrations  
22 using a chemical transport model with Moderate Resolution Imaging Spectroradiometer  
23 (MODIS) aerosol observations over East Asia, *J. Geophys. Res.-Atmos.*, 114, D04204,  
24 doi:10.1029/2008JD011041, 2009.
- 25 Chu, D. A., Kaufman, Y. J., Zibordi, G., Chern, J. D., Mao, J., Li, C. C., and Holben, B. N.:  
26 Global monitoring of air pollution over land from the Earth Observing System-Terra  
27 Moderate Resolution Imaging Spectroradiometer (MODIS), *J. Geophys. Res.-Atmos.*, 108,  
28 4661, Doi 10.1029/2002jd003179, 2003.

1 Dubovik, O., Holben, B. N., Eck, T. F., Smirnov, A., Kaufman, Y. J., King, M. D., Tanr'e, D.,  
2 and Slutsker, I.: Variability of absorption and optical properties of key aerosol types observed  
3 in worldwide locations, *J. Atmos. Sci.*, 59, 590–608, 2002.

4 Dubovik, O., Smirnov, A., Holben, B., King, M. D., Kaufman, Y. J., Eck, T. F., and Slutsker,  
5 I. Accuracy assessments of aerosol optical properties retrieved from Aerosol Robotic Network  
6 (AERONET) Sun and sky radiance measurements, *J. Geophys. Res.-Atmos.*, 105, 9791–9806,  
7 2000.

8 Dubovik, O. and King, M. D.: A flexible inversion algorithm for retrieval of aerosol optical  
9 properties from Sun and sky radiance measurements, *J. Geophys. Res.-Atmos.*, 105, 20673-  
10 20696, Doi 10.1029/2000jd900282, 2000.

11 Dubovik, O., Smirnov, A., Holben, B. N., King, M. D., Kaufman, Y. J., Eck, T. F., and  
12 Slutsker, I.: Accuracy assessments of aerosol optical properties retrieved from Aerosol  
13 Robotic Network (AERONET) Sun and sky radiance measurements, *J. Geophys. Res.-*  
14 *Atmos.*, 105, 9791-9806, Doi 10.1029/2000jd900040, 2000.

15 Emili, E., Popp, C., Petitta, M., Riffler, M., Wunderle, S., and Zebisch, M.: PM10 remote  
16 sensing from geostationary SEVIRI and polar-orbiting MODIS sensors over the complex  
17 terrain of the European Alpine region, *Remote Sens. Environ.*, 114, 2485-2499, DOI  
18 10.1016/j.rse.2010.05.024, 2010.

19 Engel-Cox, J. A., Holloman, C. H., Coutant, B. W., and Hoff, R. M.: Qualitative and  
20 quantitative evaluation of MODIS satellite sensor data for regional and urban scale air quality,  
21 *Atmos. Environ.*, 38, 2495-2509, DOI 10.1016/j.atmosenv.2004.01.039, 2004.

22 Engel-Cox, J. A., Hoff, R. M., Rogers, R., Dimmick, F., Rush, A. C., Szykman, J. J., Al-  
23 Saadi, J., Chu, D. A., and Zell, E. R.: Integrating lidar and satellite optical depth with ambient  
24 monitoring for 3-dimensional particulate characterization, *Atmos. Environ.*, 40, 8056-8067,  
25 DOI 10.1016/j.atmosenv.2006.02.039, 2006.

26 Escribano, J., Gallardo, L., Rondanelli, R., and Choi, Y.-S.: Satellite retrievals of aerosol  
27 optical depth over a subtropical urban area: the role of stratification and surface reflectance,  
28 *Aerosol. Air. Qual. Res.*, 14, 596-U568, 2014.

29 Guo, J.-P., Zhang, X.-Y., Che, H.-Z., Gong, S.-L., An, X., Cao, C.-X., Guang, J., Zhang, H.,  
30 Wang, Y.-Q., and Zhang, X.-C.: Correlation between PM concentrations and aerosol optical  
31 depth in eastern China, *Atmos. Environ.*, 43, 5876-5886, 2009.

1 Gupta, P. and Christopher, S. A.: Seven year particulate matter air quality assessment from  
2 surface and satellite measurements, *Atmos. Chem. Phys.*, 8, 3311-3324, 2008.

3 Hauck, H., Berner, A., Gomiscek, B., Stopper, S., Puxbaum, H., Kundi, M., and Preining, O.:  
4 On the equivalence of gravimetric PM data with TEOM and beta-attenuation measurements,  
5 *J. Aerosol Sci.*, 35, 1135-1149, DOI 10.1016/j.aerosci.2004.04.004, 2004.

6 Holben, B. N., Eck, T. F., Slutsker, I., Tanre, D., Buis, J. P., Setzer, A., Vermote, E., Reagan,  
7 J. A., Kaufman, Y. J., Nakajima, T., Lavenu, F., Jankowiak, I., and Smirnov, A.: AERONET -  
8 A federated instrument network and data archive for aerosol characterization, *Remote Sens.*  
9 *Environ.*, 66, 1-16, Doi 10.1016/S0034-4257(98)00031-5, 1998.

10 IPCC (Intergovernmental Panel on Climate Change): Climate Change 2013: The Physical  
11 Science Basis. Contribution of Working Group I to the Fifth Assessment Report of the  
12 Intergovernmental Panel on Climate Change, Cambridge University Press, Cambridge, United  
13 Kingdom and New York, NY, USA, 2013

14 Kappos, A. D., Bruckmann, P., Eikmann, T., Englert, N., Heinrich, U., Hoppe, P., Koch, E.,  
15 Krause, G. H. M., Kreyling, W. G., Rauchfuss, K., Rombout, P., Schulz-Klemp, V., Thiel, W.  
16 R., and Wichmann, H. E.: Health effects of particles in ambient air, *Int. J. Hyg. Environ.*  
17 *Health*, 207, 399-407, Doi 10.1078/1438-4639-00306, 2004.

18 Kaufman, Y. J., Tanré, D., and Boucher, O.: A satellite view of aerosols in the climate system,  
19 *Nature*, 419, 215-223, 2002.

20 Kim, J., Lee, J., Lee, H. C., Higurashi, A., Takemura, T., and Song, C. H.: Consistency of the  
21 aerosol type classification from satellite remote sensing during the Atmospheric Brown  
22 Cloud–East Asia Regional Experiment campaign, *J. Geophys. Res.-Atmos.*, 112, D22S33,  
23 doi:10.1029/2006JD008201, 2007.

24 Kim, S.-W., Yoon, S.-C., Kim, J., and Kim, S.-Y.: Seasonal and monthly variations of  
25 columnar aerosol optical properties over east Asia determined from multi-year MODIS,  
26 LIDAR, and AERONET Sun/sky radiometer measurements, *Atmos. Environ.*, 41, 1634-1651,  
27 DOI 10.1016/j.atmosenv.2006.10.044, 2007.

28 Koelemeijer, R. B. A., Homan, C. D., and Matthijsen, J.: Comparison of spatial and temporal  
29 variations of aerosol optical thickness and particulate matter over Europe, *Atmos. Environ.*,  
30 40, 5304-5315, DOI 10.1016/j.atmosenv.2006.04.044, 2006.

1 Kumar, N., Chu, A., and Foster, A.: An empirical relationship between PM<sub>2.5</sub> and aerosol  
2 optical depth in Delhi Metropolitan, *Atmos. Environ.*, 41, 4492-4503, 2007.

3 Lee, J., Kim, J., Song, C. H., Kim, S. B., Chun, Y., Sohn, B. J., and Holben, B. N.:  
4 Characteristics of aerosol types from AERONET sunphotometer measurements, *Atmos.*  
5 *Environ.*, 44, 3110-3117, DOI 10.1016/j.atmosenv.2010.05.035, 2010.

6 Levy, R., Mattoo, S., Munchak, L., Remer, L., Sayer, A., Patadia, F., and Hsu, N.: The  
7 Collection 6 MODIS aerosol products over land and ocean, *Atmos. Meas. Tech.*, 6, 2989-  
8 3034, 2013.

9 Levy, R. C., Remer, L. A., Mattoo, S., Vermote, E. F., and Kaufman, Y. J.: Second-  
10 generation operational algorithm: Retrieval of aerosol properties over land from inversion of  
11 Moderate Resolution Imaging Spectroradiometer spectral reflectance, *J. Geophys. Res.-*  
12 *Atmos.*, 112, D13211, Doi 10.1029/2006jd007811, 2007.

13 Liu, Y., Franklin, M., Kahn, R., and Koutrakis, P.: Using aerosol optical thickness to predict  
14 ground-level PM<sub>2.5</sub> concentrations in the St. Louis area: A comparison between MISR and  
15 MODIS, *Remote Sens. Environ.*, 107, 33-44, DOI 10.1016/j.rse.2006.05.022, 2007.

16 Liu, Y., Park, R. J., Jacob, D. J., Li, Q. B., Kilaru, V., and Sarnat, J. A.: Mapping annual mean  
17 ground-level PM<sub>2.5</sub> concentrations using Multiangle Imaging Spectroradiometer aerosol  
18 optical thickness over the contiguous United States, *J. Geophys. Res.-Atmos.*, 109, D22206,  
19 Doi 10.1029/2004jd005025, 2004.

20 Liu, Y., Sarnat, J. A., Kilaru, V., Jacob, D. J., and Koutrakis, P.: Estimating ground-level  
21 PM<sub>2.5</sub> in the eastern United States using satellite remote sensing, *Environ. Sci. Technol.*, 39,  
22 3269-3278, 2005.

23 Munchak, L., Levy, R., Mattoo, S., Remer, L., Holben, B., Schafer, J., Hostetler, C., and  
24 Ferrare, R.: MODIS 3 km aerosol product: applications over land in an urban/suburban region,  
25 *Atmos. Meas. Tech.*, 6, 1747-1759, 2013.

26 Murayama, T., Sugimoto, N., Uno, I., Kinoshita, K., Aoki, K., Hagiwara, N., Liu, Z. Y.,  
27 Matsui, I., Sakai, T., Shibata, T., Arao, K., Sohn, B. J., Won, J. G., Yoon, S. C., Li, T., Zhou,  
28 J., Hu, H. L., Abo, M., Iokibe, K., Koga, R., and Iwasaka, Y.: Ground-based network  
29 observation of Asian dust events of April 1998 in east Asia, *J. Geophys. Res.-Atmos.*, 106,  
30 18345-18359, 2001.

1 Ogunjobi, K. O., Kim, Y. J., and He, Z.: Influence of the total atmospheric optical depth and  
2 cloud cover on solar irradiance components, *Atmos. Res.*, 70, 209-227, DOI  
3 10.1016/j.atmosres.2004.01.003, 2004.

4 Pan, X. L., Yan, P., Tang, J., Ma, J. Z., Wang, Z. F., Gbaguidi, A., and Sun, Y. L.:  
5 Observational study of influence of aerosol hygroscopic growth on scattering coefficient over  
6 rural area near Beijing mega-city, *Atmos. Chem. Phys.*, 9, 7519-7530, 2009.

7 Pelletier, B., Santer, R., and Vidot, J.: Retrieving of particulate matter from optical  
8 measurements: A semiparametric approach, *J. Geophys. Res.-Atmos.*, 112, D06208., 2007.

9 Pope, C. A., Burnett, R. T., Thun, M. J., Calle, E. E., Krewski, D., Ito, K., and Thurston, G.  
10 D.: Lung cancer, cardiopulmonary mortality, and long-term exposure to fine particulate air  
11 pollution, *JAMA-J. Am. Med. Assoc.*, 287, 1132-1141, 2002.

12 Remer, L. A., Kaufman, Y. J., Tanre, D., Mattoo, S., Chu, D. A., Martins, J. V., Li, R. R.,  
13 Ichoku, C., Levy, R. C., Kleidman, R. G., Eck, T. F., Vermote, E., and Holben, B. N.: The  
14 MODIS aerosol algorithm, products, and validation, *J. Atmos. Sci.*, 62, 947-973, 2005.

15 Schaap, M., Apituley, A., Timmermans, R. M. A., Koelemeijer, R. B. A., and de Leeuw, G.:  
16 Exploring the relation between aerosol optical depth and PM<sub>2.5</sub> at Cabauw, the Netherlands,  
17 *Atmos. Chem. Phys.*, 9, 909-925, 2009.

18 Schuster, G. L., Dubovik, O., and Holben, B. N.: Angstrom exponent and bimodal aerosol  
19 size distributions, *J. Geophys. Res.*, 111, D07207, doi:10.1029/2005JD006328, 2006.

20 Song, C.-K., Ho, C.-H., Park, R. J., Choi, Y.-S., Kim, J., Gong, D.-Y., and Lee, Y.-B.: Spatial  
21 and seasonal variations of surface PM<sub>10</sub> concentration and MODIS aerosol optical depth over  
22 China, *Asia. Pac. J. Atmos. Sci.*, 45, 33-43, 2009.

23 van Donkelaar, A., Martin, R. V., Brauer, M., Kahn, R., Levy, R., Verduzco, C., and  
24 Villeneuve, P. J.: Global estimates of ambient fine particulate matter concentrations from  
25 satellite-based aerosol optical depth: development and application, *Environ. Health. Persp.*,  
26 118, 847, 2010.

27 Wang, J., and Christopher, S. A.: Intercomparison between satellite-derived aerosol optical  
28 thickness and PM<sub>2.5</sub> mass: Implications for air quality studies, *Geophys. Res. Lett.*, 30, 2095,  
29 Doi 10.1029/2003gl018174, 2003.



- 1 Wang, Z. F., Chen, L. F., Tao, J. H., Zhang, Y., and Su, L.: Satellite-based estimation of  
2 regional particulate matter (PM) in Beijing using vertical-and-RH correcting method, *Remote*  
3 *Sens. Environ.*, 114, 50-63, DOI 10.1016/j.rse.2009.08.009, 2010.
- 4 WHO (World Health Organization): WHO Air quality guidelines for particulate matter, ozone,  
5 nitrogen dioxide and sulfur dioxide - global update 2005, WHO Press, World Health  
6 Organization, Geneva, Switzerland, 2005.
- 7

1 Table 1. Previous studies associated with the estimation of PM concentrations using AOD.

Method	Study area	Data		R	Reference
		AOD	PM <sub>x</sub>		
MT1 <sup>a</sup>	Northern Italy	Daily Sunphotometer	Daily PM10	0.82	Chu et al. (2003)
MT1	Alabama	MODIS (10km)	PM2.5	0.70	Wang and Christopher. (2003)
MT1	Southeastern U.S.	MODIS (10km)	PM2.5	0.40	Engel-Cox et al. (2004)
			Daily PM2.5	0.43	
MT1	U.S.	MODIS	PM2.5	0.52	Gupta and Christopher. (2008)
			Daily PM2.5	0.62	
MT1	Cabauw	Sunphotometer	PM2.5	0.75	Schaap et al. (2009)
		MODIS (10km)		0.72	
MT2 <sup>b</sup>	Europe	MODIS (10km)	PM2.5	0.60	Koelemeijer et al. (2006)
			PM10	0.50	
MT2	Alpine region	SEVIRI	Daily PM10	0.70	Emili et al. (2010)
		MODIS		0.60	
MT2	Beijing	MODIS (1km)	PM2.5	0.68	Wang et al. (2010)
			PM10	0.68	
MT3 <sup>c</sup>	Eastern U.S.	MISR	Daily PM2.5	0.69	Liu et al. (2005)
MT3	St. Louis	MISR	Daily PM2.5	0.79	Liu et al. (2007)
		MODIS		0.71	
MT3	Lille	Sunphotometer	PM10	0.87	Pelletier et al. (2007)
MT4 <sup>d</sup>	U.S.	MISR	Yearly PM2.5	0.78	Liu et al. (2004)
MT4 <sup>d</sup>	East Asia	MODIS	Seasonal PM10	0.28-0.54	Choi et al. (2009)

2 <sup>a</sup> MT1 uses the empirical linear relationship between AOD and PM<sub>x</sub> ( $PM_x = aAOD + b$ ).

3 <sup>b</sup> MT2 uses the empirical linear relationship between corrected AOD (vertical distribution,  
4 RH) and PM<sub>x</sub>.

5 <sup>c</sup> MT3 uses the poly-parameter model.

6 <sup>d</sup> MT4 uses the 3D atmospheric chemistry model.

1 Table 2. Statistical summary of AOD and cloud screened AOD (AOD<sub>cl</sub>) observed by  
 2 AERONET and MODIS during the DRAGON-Asia campaign period.

	AERONET		MODIS	
	AOD	AOD <sub>cl</sub>	AOD	AOD <sub>cl</sub>
Mean ± std	0.51 ± 0.34	0.42 ± 0.26	0.74 ± 0.38	0.73 ± 0.37
Min	0.09	0.09	0.03	0.03
Median	0.43	0.35	0.72	0.68
Max	2.99	1.42	1.94	1.94
N	3406	2112	292	252

3

1 Table 3. The empirical linear models used for PM10 estimations in this study.

Model	Model description	Application
M1	$PM_{10} = aAOD + b$	AERONET, MODIS
M2	$PM_{10} = a \frac{AOD}{BLH} + b$	AERONET, MODIS
M3	$PM_{10} = a \frac{AOD \times R_{eff}}{BLH} + b$	AERONET
M4	$PM_{10} = a \frac{AOD}{BLH \times f(RH)} + b$	AERONET, MODIS
M5	$PM_{10} = a \frac{AOD \times R_{eff}}{BLH \times f(RH)} + b$	AERONET
M6	Section 3.2 Eq. (5) (multiple linear regression model)	AERONET

2

1 Table 4. Estimated regression coefficients for the multiple linear regression model (M6)  
 2 (described in Section 3.2, Eq. (5)) using AERONET data (N = 1058).

Model parameter	Estimate	Standard error	<i>P</i> value
Intercept	4.363	0.080	< 0.0001
ln(AOD)	0.527	0.022	< 0.0001
ln(BLH)	-0.280	0.028	< 0.0001
ln(AE)	0.066	0.033	0.047
Location type			
Near source	0.233	0.032	< 0.0001
Urban	0.013	0.032	0.684
Suburban	0.000	-	-
Wind speed	0.015	0.008	0.052
Wind direction			
From the north	0.205	0.054	< 0.0001
From the south	0.164	0.045	< 0.0001
From the west	0.307	0.036	< 0.0001
From the east	0.000	-	-
RH	-0.610	0.116	< 0.0001
Temperature	-0.010	0.002	< 0.0001

3

1 Table 5. Correlation coefficient (R), root mean square error (RMSE), mean normalized bias  
 2 (MNB), and mean fractionalized bias (MFB) between measured and PM10 concentrations and  
 3 those estimated by the different empirical linear models, using AERONET and MODIS data,  
 4 during the DRAGON-Asia campaign period in Seoul. Numbers in parentheses represent  
 5 results corresponding to the same number of data points as used in M3 and M5, when  
 6 effective radius of aerosol data were available.

		Model						
		M1	M1 <sub>cl</sub>	M2	M3	M4	M5	M6
AERONET	R	0.40	0.54	0.62 (0.46)	0.55	0.63 (0.47)	0.58	0.68
	R <sup>2</sup>	0.16	0.29	0.39 (0.21)	0.30	0.40 (0.23)	0.34	0.47
	N	1712	1054	1054 (373)	373	1054 (373)	373	1054
	RMSE (μg/m <sup>3</sup> ) <sup>a</sup>	28.62	23.79	22.11 (23.27)	22.01	22.11 (22.98)	21.32	21.05
	MNB (%) <sup>b</sup>	27.70	21.75	21.27 (25.39)	22.11	21.27 (24.54)	20.66	5.65
	MFB (%) <sup>c</sup>	10.96	9.20	8.97 (10.43)	9.08	8.97 (10.17)	8.50	-0.83
MODIS	R	0.46	0.50	0.72	-	0.71	-	-
	R <sup>2</sup>	0.21	0.25	0.51	-	0.51	-	-
	N	291	252	252	-	252	-	-
	RMSE (μg/m <sup>3</sup> )	28.49	28.55	23.02	-	23.19	-	-
	MNB (%)	22.09	21.83	14.80	-	14.92	-	-
	MFB (%)	9.53	9.64	6.40	-	6.53	-	-

7 <sup>a</sup> RMSE (Root mean square error) =  $\sqrt{\frac{1}{N} \sum_{i=1}^N (m_i - o_i)^2}$

8 <sup>b</sup> MNB (Mean normalized bias) =  $\frac{1}{N} \sum_{i=1}^N \frac{(m_i - o_i)}{o_i} \times 100\%$

9 <sup>c</sup> MFB (Mean fractionalized bias) =  $\frac{1}{N} \sum_{i=1}^N \frac{(m_i - o_i)}{\left(\frac{m_i + o_i}{2}\right)} \times 100\%$

10  $m_i$  and  $o_i$  indicate estimated PM10 using models and observed PM10 concentrations,  
 11 respectively. N is the number of data points.

12

1 Table 6. Spatial variations of the correlation coefficient (R), root mean square error (RMSE),  
 2 mean normalized bias (MNB), and mean fractionalized bias (MFB) between measured PM10  
 3 concentrations and those estimated from the different empirical linear models for the three  
 4 different site categories, using the data collected by AERONET and MODIS, during the  
 5 DRAGON-Asia campaign period in Seoul.

		Performance of empirical models used to estimate hourly PM10 using AERONET datasets with respect to model and measurement site types					
		Model					
		M1 <sub>el</sub>	M2	M3	M4	M5	M6
NS	R	0.49	0.57 (0.49)	0.59	0.57 (0.49)	0.61	0.61
	R <sup>2</sup>	0.24	0.32 (0.24)	0.35	0.33 (0.24)	0.38	0.37
	N	807	807 (237)	237	807 (237)	237	190
	RMSE (µg/m <sup>3</sup> )	26.29	24.79 (26.90)	24.79	24.67 (26.79)	24.28	22.85
	MNBE (%)	21.21	20.54 (27.32)	24.57	20.38 (26.95)	23.48	7.12
	MFB (%)	9.03	8.56 (15.21)	13.05	8.65 (15.05)	12.35	-0.37
TU	R	0.51	0.60 (0.43)	0.61	0.61 (0.45)	0.64	0.72
	R <sup>2</sup>	0.26	0.36 (0.18)	0.37	0.37 (0.20)	0.42	0.51
	N	891	891 (367)	367	891 (367)	367	190
	RMSE (µg/m <sup>3</sup> )	22.61	21.11 (21.77)	19.06	20.94 (21.50)	18.43	17.69
	MNBE (%)	24.27	24.25 (23.91)	20.26	23.47 (22.67)	18.46	4.16
	MFB (%)	10.09	9.84 (6.14)	5.39	9.88 (5.78)	4.86	-1.85
RA	R	0.63	0.73 (0.63)	0.69	0.73 (0.64)	0.70	0.76
	R <sup>2</sup>	0.40	0.53 (0.40)	0.47	0.54 (0.42)	0.50	0.59
	N	414	414 (109)	109	414 (109)	109	92
	RMSE (µg/m <sup>3</sup> )	19.67	17.35 (18.02)	16.92	17.26 (17.81)	16.53	17.09
	MNBE (%)	17.31	16.08 (25.85)	22.60	15.32 (25.19)	21.52	5.99
	MFB (%)	8.15	7.26 (13.61)	12.08	6.94 (13.41)	11.62	0.47

Performance of empirical models to estimate hourly PM10 using MODIS datasets with respect to model and measurement site types

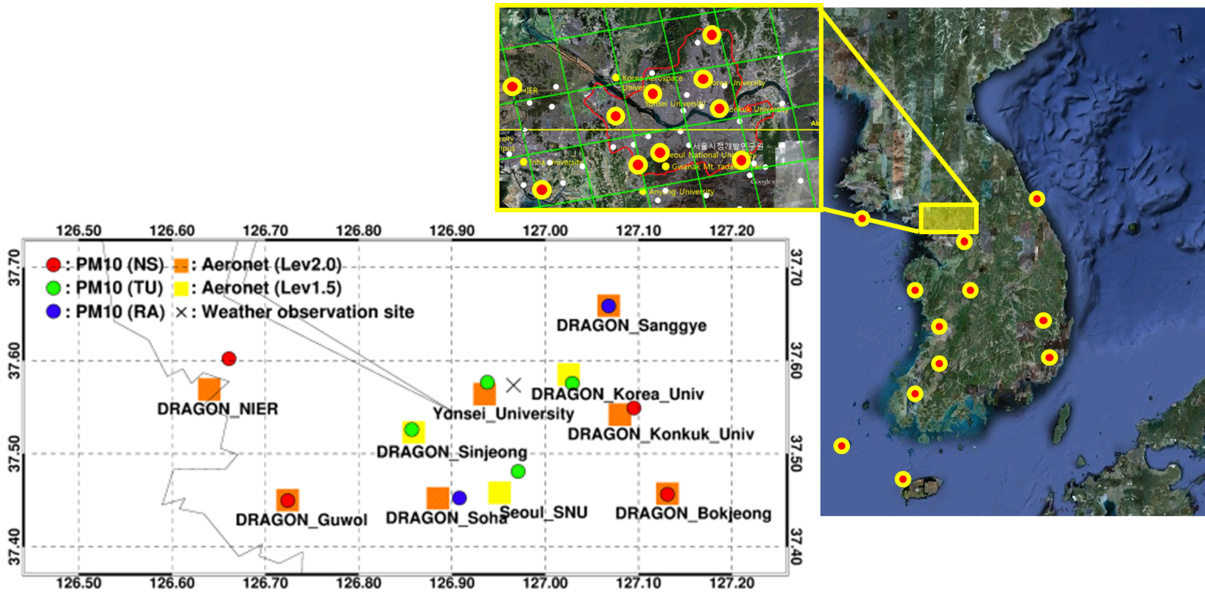
		Model					
		M1 <sub>cl</sub>	M2	M3	M4	M5	M6
NS	R	0.37	0.68	-	0.68	-	-
	R <sup>2</sup>	0.14	0.46	-	0.46	-	-
	N	105	105	-	105	-	-
	RMSE (µg/m <sup>3</sup> )	32.09	27.34	-	27.32	-	-
	MNBE (%)	24.93	16.10	-	15.98	-	-
	MFB (%)	10.80	6.99	-	7.04	-	-
TU	R	0.42	0.72	-	0.71	-	-
	R <sup>2</sup>	0.18	0.52	-	0.50	-	-
	N	95	95	-	95	-	-
	RMSE (µg/m <sup>3</sup> )	26.41	20.08	-	20.45	-	-
	MNBE (%)	21.23	15.23	-	15.58	-	-
	MFB (%)	9.42	6.55	-	6.78	-	-
RA	R	0.50	0.76	-	0.74	-	-
	R <sup>2</sup>	0.25	0.57	-	0.55	-	-
	N	52	52	-	52	-	-
	RMSE (µg/m <sup>3</sup> )	23.66	17.93	-	18.33	-	-
	MNBE (%)	17.36	11.40	-	11.57	-	-
	MFB (%)	7.96	4.93	-	5.04	-	-



1 Table 7. Seasonal variations of the correlation coefficient (R) and root mean square error  
 2 (RMSE) between measured PM10 concentrations and those estimated by the different  
 3 empirical linear models using AERONET datasets, collected at Yonsei University for 17  
 4 months.

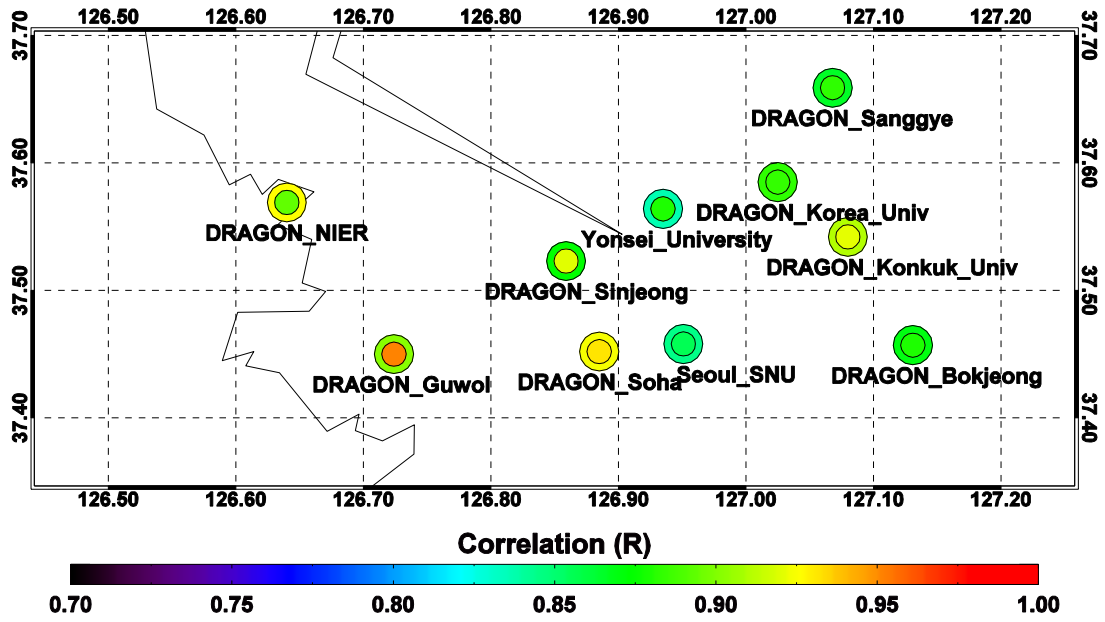
Performance of empirical models to estimate hourly PM10 using AERONET datasets with respect to model and season						
		Model				
		M1 <sub>cl</sub>	M2	M3	M4	M5
Spring	R	0.39	0.47 (0.45)	0.48	0.48 (0.46)	0.54
	R <sup>2</sup>	0.15	0.22 (0.20)	0.24	0.23 (0.21)	0.29
	N	465	465 (142)	142	465 (142)	142
	RMSE (μg/m <sup>3</sup> )	41.17	39.60 (29.39)	28.77	39.37 (29.16)	27.76
Summer	R	0.70	0.67 (0.64)	0.64	0.71 (0.67)	0.66
	R <sup>2</sup>	0.50	0.46 (0.41)	0.41	0.50 (0.45)	0.43
	N	85	85 (21)	21	85 (21)	21
	RMSE (μg/m <sup>3</sup> )	13.85	14.39 (13.75)	13.60	13.81 (13.13)	10.39
Autumn	R	0.60	0.64 (0.52)	0.54	0.66 (0.57)	0.58
	R <sup>2</sup>	0.36	0.42 (0.28)	0.29	0.41 (0.33)	0.34
	N	212	212 (99)	99	212 (99)	99
	RMSE (μg/m <sup>3</sup> )	13.41	12.89 (14.86)	14.71	12.66 (14.32)	14.17
Winter	R	0.63	0.70 (0.70)	0.81	0.70 (0.70)	0.81
	R <sup>2</sup>	0.40	0.49 (0.49)	0.65	0.49 (0.49)	0.66
	N	284	284 (116)	116	284 (116)	116
	RMSE (μg/m <sup>3</sup> )	19.81	18.17 (21.16)	17.44	18.10 (21.01)	17.29

5



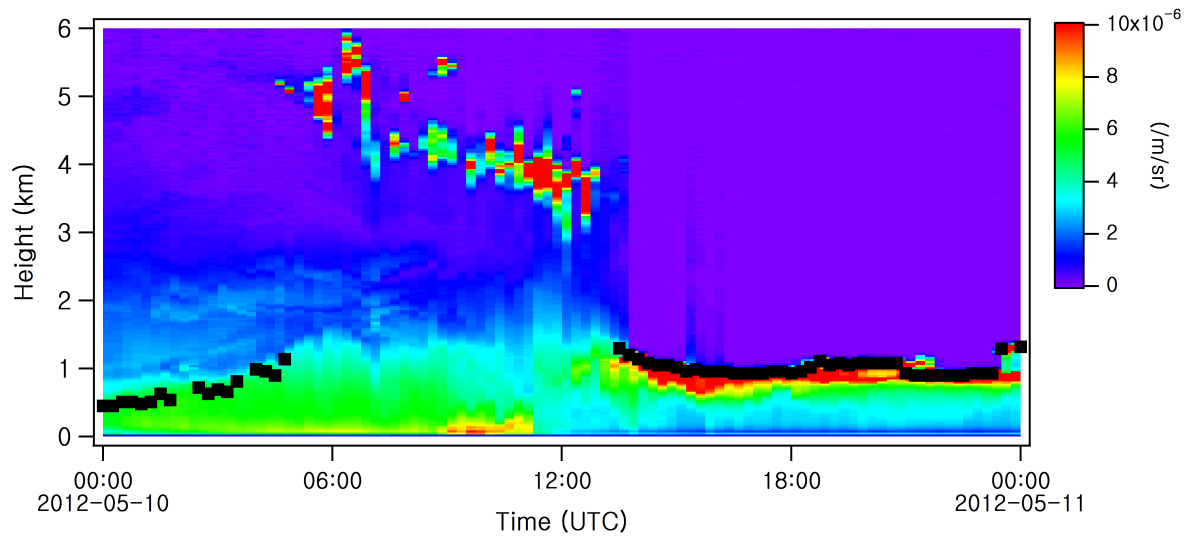
1  
2  
3  
4  
5  
6  
7  
8

Figure 1. The spatial distribution of AERONET stations, PM10 monitoring sites, and weather observation sites across the Seoul metropolitan area. Orange and yellow boxes indicate the locations of AERONET level 2.0 and 1.5 sites, respectively. The colored circles denote the locations of PM10 monitoring sites. Red, green, and blue sites represent near source (NS), typical urban (TU), and residential area (RA) site types, respectively.



1  
2  
3  
4  
5  
6  
7

Figure 2. The distribution of correlation coefficients between AERONET AOD and MODIS AOD at 0.55 μm with respect to different spatial resolutions. The inner (outer) circle indicates the correlation between AERONET AOD and MODIS AOD with a resolution of 10 km (30 km).

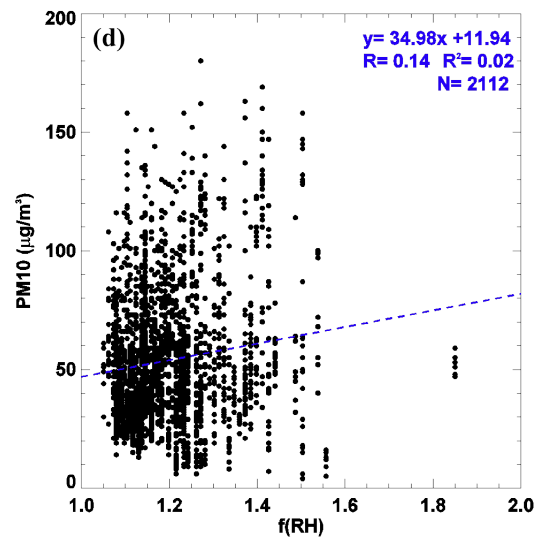
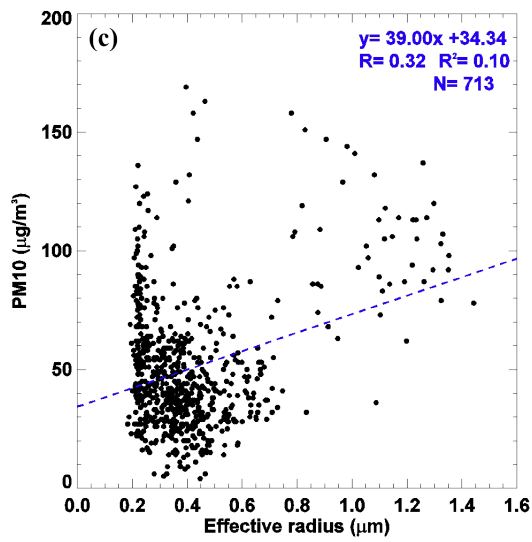
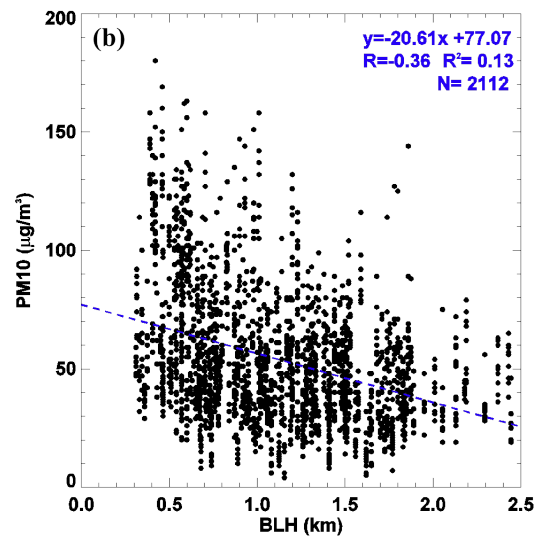
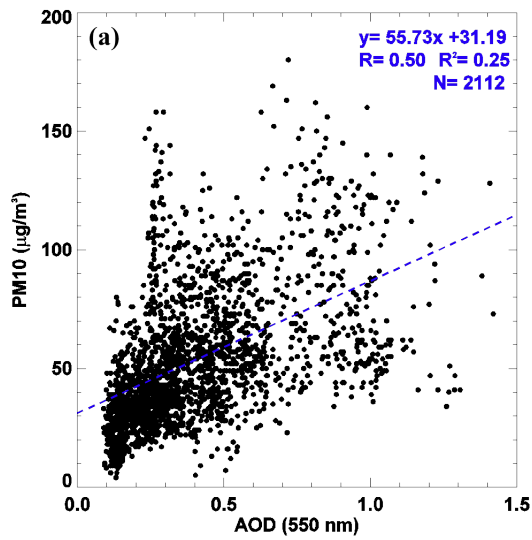


1

2

3 Figure 3. Time plot of attenuated backscatter coefficients observed from the two-wavelength  
4 Mie lidar at Seoul National University, and boundary layer height (marked by black squares)  
5 retrieved by the automated wavelet covariance transform (WCT) method of Brooks (2003).

6

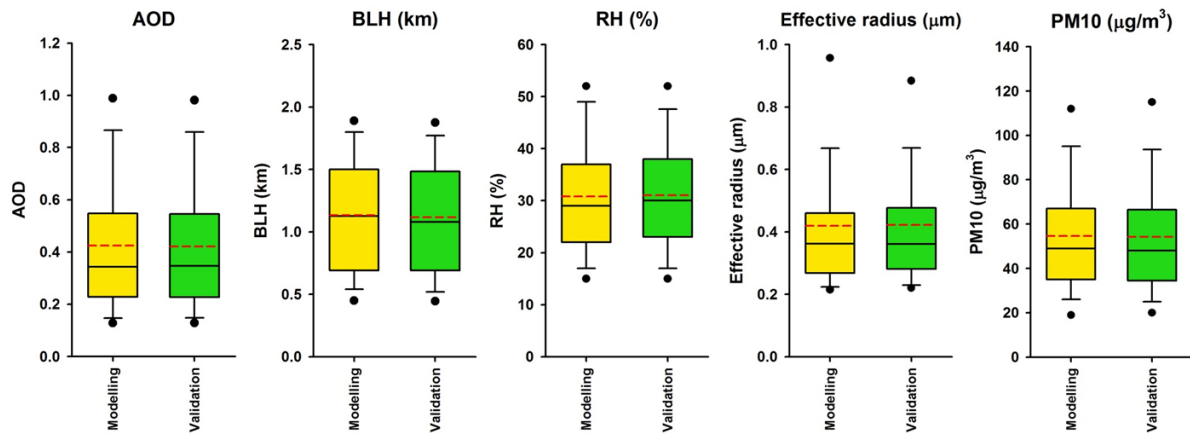


1

2

3 Figure 4. Scatter plots of the various parameters including (a) AOD, (b) BLH, (c) effective  
 4 radius, and (d) RH against the dependent variable of PM10 concentration. The regression line  
 5 is shown as a blue dashed line.

6

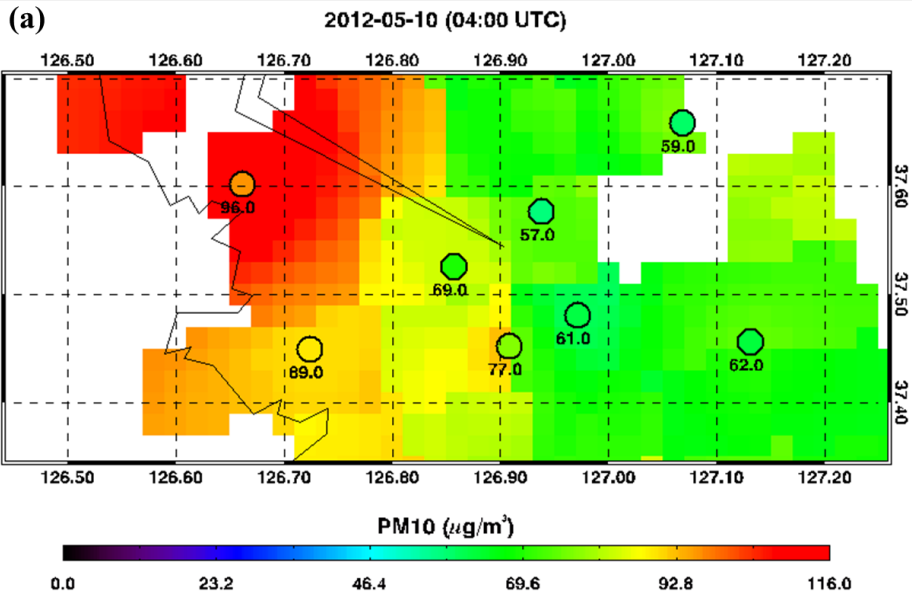


1

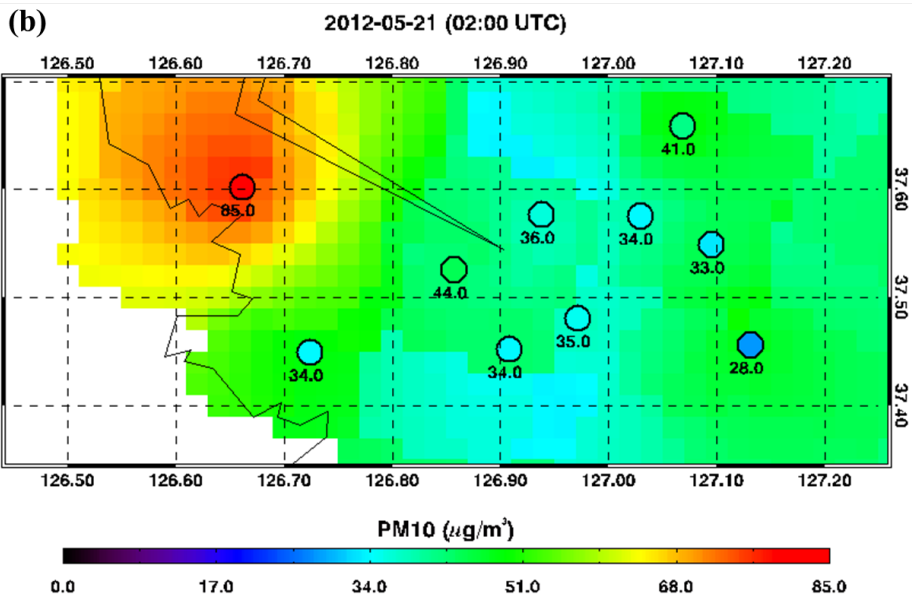
2

3 Figure 5. The distribution (5%, 10%, 25%, median, 75%, 90%, and 95%) of AOD, boundary  
 4 layer height (BLH), relative humidity (RH), effective radius, and PM10 concentrations in the  
 5 modeling and validation groups derived from AERONET datasets collected during the  
 6 DRAGON-Asia campaign in Seoul. The red dashed line in the plot denotes the mean value.

7



1



2

3

4 Figure 6. Distribution of hourly surface PM10 concentrations estimated by model M2 using  
 5 the MODIS datasets for (a) 4 UTC, 10 May, 2012 and (b) 2 UTC, 21 May, 2012. Circles  
 6 indicate the observed PM10 concentrations at PM monitoring sites.